Dalton Transactions

ROYAL SOCIETY OF CHEMISTRY

PAPER

View Article Online
View Journal | View Issue

Cite this: *Dalton Trans.*, 2021, **50**, 12006

Distinctive modulation of optical anisotropy by halogens in α/β-Cd–P–X (X = Cl, Br, and I)†

Kewang Zhang,[a] Junben Huang,[b] Zhikang Chen,[a] Bei Zhang,[a] Ming-Hsien Lee[c] and Jun Zhang *[a]

Received 9th April 2021,
Accepted 8th July 2021

DOI: 10.1039/d1dt01168e

rsc.li/dalton

Birefringent materials are widely applied as photoelectric functional field devices to modulate the polarization of lasers. The introduction of a halogen into the structure of crystals could balance the relationship between the band gap E_g and nonlinear optical (NLO) coefficient owing to their outstanding electronegativity and control the optical anisotropy. In this work, the optical properties of phosphohalides α/β-Cd_2P_3X (X = Cl, Br, I) were studied. It was found that the birefringences of α/β-Cd_2P_3Cl (0.23/0.24 @ 1064 nm) are unexpectedly 8 times larger than those of α/β-Cd_2P_3I (0.04/0.03 @ 1064 nm). To find the optical property origins and explore the contributions of microscopic groups to the optical anisotropy and NLO responses in Cd–P–X (X = Cl, Br, I), the first-principles, real-space atom-cutting, and polarizability anisotropy analysis methods were used. This reveals that the electron distribution is susceptible to halogen electronegativity. Halogen atoms can modulate the polarization anisotropy of the active polyhedron and influence the birefringence significantly, owing to the synergistic effect of the anion size and strong covalent interactions between halogens and metal cations. This work clarifies the optical anisotropy origin mechanism and provides a general strategy for finding promising birefringent crystals in phosphohalide systems.

1. Introduction

Birefringence is an essential component of the performance estimation of nonlinear optical (NLO) materials, which plays an important role in modulating light polarization, and is widely utilized in laser fields such as in optical communications, polarizing microscopic observations, and phase-matching *etc.*[1–14] After decades of unremitting efforts, a series of commercial birefringent crystal materials with excellent performance have been obtained, such as typical representatives α-BaB_2O_4,[15] YVO_4,[16] $CaCO_3$,[17] TiO_2,[18] MgF_2,[19] $Ca(BO_2)_2$ [20] and $Li_2Na_2B_2O_5$,[21] *etc.* However, they remain inadequate for meeting the growing market and technical demand; for example, $CaCO_3$ [17] and TiO_2 [18] are difficult to synthesize artificially as minerals and YVO_4 [16] has stringent growth temperature standards.

The structure–property relationship is inextricably intertwined and the microgroups of the material will determine the macroscopic properties. There is no denying that birefringence is a macroscopic manifestation of microscopic polarizability anisotropy, which could be enlarged in several ways such as by (I) introducing some functional chromophores with large optical anisotropy;[22] *e.g.*, like the coplanar and dense groups with π-conjugation systems (BO_3, B_3O_6, CO_3, $C_3N_3O_3$, *etc.*),[23–27] in $Ca_3(BO_3)_2$,[27b] α-BaB_2O_4,[15] $CaCO_3$,[17] and KLi$(HC_3N_3O_3)\cdot 2H_2O$.[28] Besides, the synergism of the anionic groups such as BO_3 + BO_3F renders apparent structural anisotropy, for instance, in the structures of $NH_4B_4O_6F$,[29] NaB_4O_6F,[30] CsB_4O_6F,[31] RbB_4O_6F, *etc.*[32] (II) adding d^0 cations (Zr^{4+}, Ti^{4+}, Nb^{5+}, V^{5+}, *etc.*)[33a] with an obvious second-order Jahn–Teller effect such as $LiNbO_3$,[33b] $KTiOPO_4$ (KTP) *etc.*;[34] (III) choosing cations with lone electron pairs (Sn^{2+}, Pb^{2+}, Bi^{3+}, As^{3+}, *etc.*) such as α-SnF_2,[35] $Sn_2B_5O_9Cl$,[36] $Sn_2B_5O_9Br$[37] *etc.*; (IV) using high polarization d^{10} cations (Hg^{2+}, *etc.*) such as $LiHgPO_4$,[38] $BaHgSe_2$,[39] and $Ag_6HgSiSe_6$ [40] *etc.*; and (V) utilizing the synergistic action of diverse chromophores, such as SbB_3O_6 [41] and $HgAsQ_4X$[22,42] (Q = S and Se; X = Cl, Br, and I). Among them, SbB_3O_6 exhibits a remarkable birefringence (Δn = 0.290 @ 546 nm) which can be attributed to the stereochemically active lone pair (SCALP) cations Sb^{3+} and the B–O anionic groups. In $HgAsQ_4X$ (Q = S, Se; X = Cl, Br, and I), the synergistic effect of the d^{10} cation Hg^{2+}, the SCALP cation As^{3+} and the

[a]*School of Physics Science and Technology, Xinjiang University, Urumqi 830046, Xinjiang, People's Republic of China. E-mail: zhj@xju.edu.cn*
[b]*School of Materials Science and Engineering, Education Ministry Key Laboratory of Non-ferrous Materials Science and Engineering, Central South University, Changsha 410083, Hunan, China*
[c]*Department of Physics, Tamkang University, New Taipei 25137, Taiwan*

† Electronic supplementary information (ESI) available: Table of crystal structure information, calculated optical permittivities $\Delta\varepsilon$, the data of Born effective charges, calculated band gap and PDOS, the NLO coefficients, the SHG response origins, and the electron-density difference maps. See DOI: 10.1039/d1dt01168e

mixed anions Q^{2-}/X^{-} co-determine their birefringence. In addition, recent research has shown that the strong interactions between the O_2^{2-} anions and the V^{5+} 3d orbitals in $Rb_2VO(O_2)_2F$ have a significant effect on birefringence.[43] However, the mechanism of halogen regulation of birefringence is not immediately available.

In this paper, the origin of the optical properties of α/β-Cd_2P_3X (X = Cl, Br, and I)[44] has been explored by multiple analysis methods. Experimental birefringences are hardly obtained because of the difficulties in growing large crystals but could be easily calculated from dielectric functions by the first-principles method. Based on the available Born effective charges,[45–48] a larger Δq index of X (X = Cl, Br, and I) reflects a larger influence on polarization. Through polarizability anisotropy analysis,[23] it is found that the halogen atoms lead to different birefringences of the title compounds by modulating the polarizability anisotropy of the polyhedral active group elements due to the synergistic effect of the anion size and covalent interactions.

2. Computational details

Electronic structures and optical properties of the target compounds were calculated by first-principles calculations based on the density-functional theory (DFT) method[49] implemented in the CASTEP package.[50] The Perdew–Burke–Ernzerhof (PBE) exchange–correlation functional[51] was used within the generalized gradient approximation (GGA). The norm-conserving pseudopotentials (NCPs)[52] were selected for structural optimization and calculating the electronic and optical properties. The following electronic configurations were treated: Cd $4p^6 4d^{10} 5s^2$, Hg $5p^6 5d^{10} 6s^2$, P $3s^2 3p^3$, Cl $3s^2 3p^5$, Br $4s^2 4p^5$, and I $5s^2 5p^5$; the cutoff energy was set to 830 eV for α/β-Cd_2P_3Cl and Hg_2P_3Cl, 660 eV for α/β-Cd_2P_3Br, α/β-Cd_2P_3I, and Hg_2P_3Br, respectively. Furthermore, to reach the convergence of this calculation, the Brillouin zone comprised a 3 × 3 × 3 Monkhorst–Pack *k*-point sampling with a separation of 0.025 $Å^{-1}$. The other calculation parameters and convergent criteria used were the default values of the CASTEP code.

The so-called length-gauge formalism derived by Aversa and Sipe[53] was adopted. At a zero frequency, the static second-order nonlinear susceptibilities can be ascribed to the virtual-hole (VH) and virtual-electron (VE) processes. The formulas for calculating the contributions from VE and VH are as follows:[54]

$$\chi^{(2)}_{\alpha\beta\gamma} = \chi^{(2)}_{\alpha\beta\gamma}(\mathrm{VH}) + \chi^{(2)}_{\alpha\beta\gamma}(\mathrm{VE})$$

where,

$$\chi^{(2)}_{\alpha\beta\gamma}(\mathrm{VH}) = \frac{e^3}{2\hbar^2 m^3}\sum_{vv'c}\int\frac{d^3k}{4\pi^3}P(\alpha\beta\gamma)\mathrm{Im}[p^{\alpha}_{vv'}p^{\beta}_{v'c}p^{\gamma}_{cv}] \times\left(\frac{1}{\omega^3_{cv}\omega^2_{v'c}}+\frac{2}{\omega^4_{vc}\omega_{cv'}}\right)$$

$$\chi^{(2)}_{\alpha\beta\gamma}(\mathrm{VE}) = \frac{e^3}{2\hbar^2 m^3}\sum_{vcc'}\int\frac{d^3k}{4\pi^3}P(\alpha\beta\gamma)\mathrm{Im}[p^{\alpha}_{vc}p^{\beta}_{cc'}p^{\gamma}_{c'v}] \times\left(\frac{1}{\omega^3_{cv}\omega^2_{vc'}}+\frac{2}{\omega^4_{vc}\omega_{c'v}}\right)$$

Here, α, β, and γ are Cartesian components, v and v' denote the valence bands, c and c' denote the conduction bands, and $P(\alpha\beta\gamma)$ denotes full permutation. The band energy difference and momentum matrix elements are denoted as $\hbar\omega_{ij}$ and P^{α}_{ij}, respectively.

3. Results and discussion

3.1. Crystal and electronic structure

By investigating the inorganic crystal structure database (ICSD, Version 4.5.0, build 20201130-0717), eight cadmium/mercury phosphohalides $M^{d10}{}_2P_3X$ (M^{d10} = Cd and Hg; X = Cl, Br, and I) were screened. Among them, cadmium phosphohalides have two phases, namely α/β-Cd_2P_3X (X = Cl, Br, and I), which crystallize in the space groups of *Cc* and *C*2/*c*, respectively. The space groups of Hg_2P_3Cl and Hg_2P_3Br[55] are *C*2/*c* and *Pbcn*, respectively. For α-Cd_2P_3Cl, the Cd atoms are coordinated tetrahedrally to three P atoms and one Cl atom, while in α-Cd_2P_3Br and α-Cd_2P_3I, each Cd atom bonds with two equivalent halogen atoms and three P atoms, forming a distorted triangular-bionic structure (Fig. 1c). In both phases, the Cd–P bonds form one-dimensional helical chains along the *c*-axis (Fig. 1b), and the P–P bond bridges the neighboring helical chains into a three-dimensional structure (Fig. 1a). Meanwhile, relative to the *Cc* space group, there is only one position for Cd in the β-Cd_2P_3X phase of the *C*2/*c* group, and the rest of the frame is approximately the same. Moreover, different halogen atoms exhibit diverse coordination environments, namely Cl is linked to two Cd to constitute a zero-dimensional (0D) isolated group, while Br and I are connected to four Cd in the *ab* plane as 2D layers.

The electronic structures of the title compounds were calculated using the GGA and HSE06 hybrid functionals[56,57] (listed in Table S2†). They are all indirect gap materials with calculated band gaps (HSE06) of α-Cd_2P_3Cl (1.99), α-Cd_2P_3Br (1.93), α-Cd_2P_3I (1.85), β-Cd_2P_3Cl (1.98), β-Cd_2P_3Br (1.91), β-Cd_2P_3I (1.89), Hg_2P_3Cl (1.86), and Hg_2P_3Br (1.71 eV), respectively (Fig. S1†), which are larger than those calculated by the GGA method due to the discontinuity in the derivative of exchange–correlation energy within the GGA functional.[51] The band gaps obtained by the HSE06 function match better with the experimental value.[6]

The total and partial density of states of the title phosphohalides are calculated to analyze the distribution of atom orbitals in the energy range of −20 to 20 eV, as shown in Fig. S2.† Similar electronic structures are demonstrated for the target compounds. The contributions at the top of valence bands (VBs) are primarily dominated by the P 3p and Cl/Br/I 3p/4p/5p orbitals. The bottom of conduction bands (CBs) is mainly occupied by the Cd/Hg 4p/5p and P 3p orbitals. It is noted that

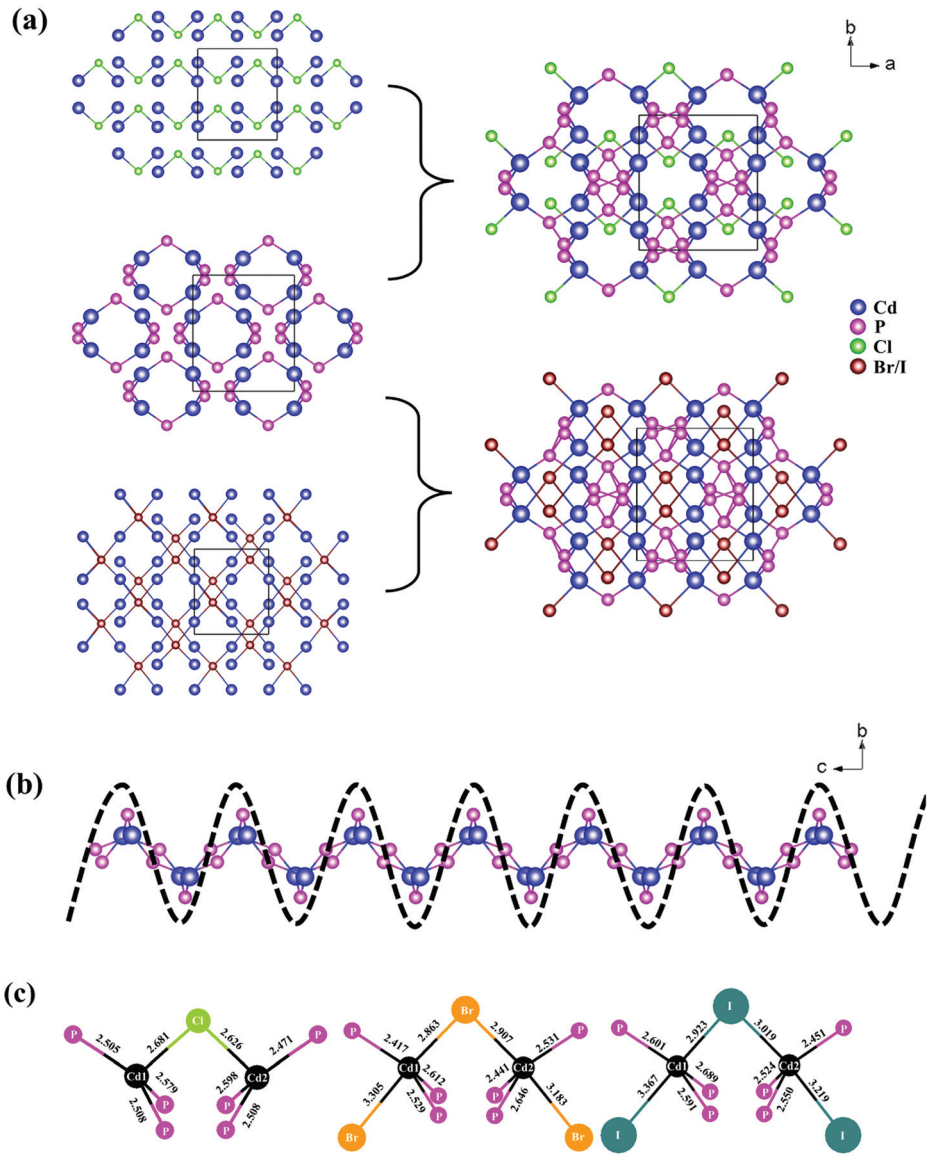

Fig. 1 Crystal structures of (a) α-Cd_2P_3X (X = Cl, Br, and I) viewed along the *c* axis. (b) The one-dimensional helical chain of Cd–P bonds. (c) The coordination environment of the Cd^{2+} cation.

the halogen and P atomic orbitals have much occupancy around the Fermi level, which means that they will play an important role in the optical properties of the title compounds.

3.2. Optical properties

The birefringences of α/β-Cd_2P_3X (X = Cl, Br, and I) crystals are estimated based on the first-principles method. The calculated birefringences of α/β-Cd_2P_3X (X = Cl, Br, and I) are given in Table S3.† In both phases, the birefringence decreases from Cl to Br to I, namely 0.24 and 0.29 for α/β-Cd_2P_3Cl, 0.19 and 0.18 for α/β-Cd_2P_3Br, and 0.04 and 0.03 for α/β-Cd_2P_3I at 1064 nm. Hg_2P_3Cl and Hg_2P_3Br exhibit moderate birefringences of about 0.09 and 0.10 at 1064 nm. In general, the polarizability anisotropy of a metal cation polyhedron has much influence on the birefringence and further halogens will affect the polarizability anisotropy of the metal cation polyhedron.[58] A series of halide crystals have been reported and their birefringences are summarized in Table S4,† including HgX_2 (X = Cl and Br),[59] Hg_2X_2 (X = Cl, Br, and I),[60] $CsEX_3$ (E = Ge and Pb; X = Cl, Br, and I),[61] $(Cu(PS_3As_3)_4)X$ (X = Cl and Br),[62] $NaSb_3X_{10}$ (X = F, Cl, Br, and I),[63] SbX_3 (X = F, Cl, Br, and I),[63b,64] and $M_2B_5O_9X$ (M = Ca, Sr, Ba, and Pb, Sn; X = Cl, Br, and I).[36,37,65] Taking $CsPbI_6$ as the example, Zhang *et al.* demonstrated that the [PbI_6] octahedral unit determines the birefringence of $CsPbI_6$ with a perovskite-like structure and the polarizability anisotropy of $CsPbX_3$ (X = Cl, Br, and I) is listed in Table S5.†[61e] Besides, among these isostructural halides, an increasing trend of birefringence from Cl to I (listed in Table S4†) could be observed, which shows a contrasting phenomenon in the title com-

pounds. Upon analyzing the polarizability anisotropy of the polyhedral, it is found that in the title compounds, from Cl to I, the calculated $\Delta\alpha$ data show a decreasing tendency (Table 1).

The NLO coefficients, SHG response origins, and the effect of halides on the NLO properties of the title compounds have also been calculated and the results are shown in the ESI.†

3.3. Origins of linear optical properties

The first-principles calculations were used to determine the refractive index values by calculating the dielectric constants ε.[66] The constants ε of uniaxial and biaxial crystals are $\begin{bmatrix} \varepsilon_1 & 0 & 0 \\ 0 & \varepsilon_1 & 0 \\ 0 & 0 & \varepsilon_3 \end{bmatrix}$ and $\begin{bmatrix} \varepsilon_1 & 0 & 0 \\ 0 & \varepsilon_2 & 0 \\ 0 & 0 & \varepsilon_3 \end{bmatrix}$, respectively. The values of the optical permittivities $\Delta\varepsilon$ of the title compounds are listed in Table S3.† It can be seen that larger dielectric constant values result in larger birefringence.

The RSAC operation was used to analyze the properties of the "changed crystal structure" by setting the band wave function as zero in the zones that belong to a specific ion or a cluster. The cutting rule follows the basic principle of "keeping the atomic spheres in contact with each other without overlapping",[67] and the cutting radii are shown in Table S6.† After cutting the halogen atoms, the residual parts in all the structures are Cd–P frameworks. However, the birefringences calculated from the remaining Cd–P frameworks show large differences, as shown in Fig. 2.

In addition, the birefringences before and after cutting the halogens change significantly, especially in α-Cd_2P_3I (from 0.04 to 0.17 @ 1064 nm), as shown in Fig. 3. The same phenomenon occurs in Hg_2P_3Cl, namely, its birefringence changed from 0.20 to 0.29, after cutting the Cl atoms in the structure, which matches well with our results. The performance is inextricably related to the microstructure.

To have deeper insights into the mechanism of the halide-induced modulation of the birefringence of Cd–P–X (X = Cl, Br, and I), Born effective charge and polarizability anisotropy analyses are applied to identify the effect of halogens on the

Table 1 Static polarization and polarization anisotropy of α/β-Cd_2P_3X (X = Cl, Br, and I) series

				Static polarization (a.u.)					
Compound	Space group	Species	$\Delta\alpha$	*xx*	*xy*	*yy*	*xz*	*yz*	*zz*
α-Cd_2P_3Cl	*Cc*	$[Cd^{I}P_3Cl]$	125.47	170.94	−68.88	155.78	−14.66	13.18	176.52
		$[Cd^{II}P_3Cl]$	124.48	170.56	68.19	159.40	−9.97	−18.14	177.97
α-Cd_2P_3Br	*Cc*	$[Cd^{I}P_3Br_2]$	103.28	178.49	−58.23	172.79	−3.46	11.66	180.76
		$[Cd^{II}P_3Br_2]$	104.29	198.74	50.03	185.54	−22.47	−23.60	184.96
α-Cd_2P_3I	*Cc*	$[Cd^{I}P_3I_2]$	45.89	206.99	−16.71	204.64	−11.31	13.95	188.61
		$[Cd^{II}P_3I_2]$	62.63	205.50	29.18	214.31	−6.98	−15.47	188.80
β-Cd_2P_3Cl	*C*2/*c*	$[CdP_3Cl]$	118.95	171.71	−65.15	161.24	−12.35	16.09	176.36
β-Cd_2P_3Br	*C*2/*c*	$[CdP_3Br_2]$	85.86	199.78	−44.62	193.16	−10.25	16.78	182.10
β-Cd_2P_3I	*C*2/*c*	$[CdP_3I_2]$	59.84	212.07	−26.88	211.55	−10.05	14.32	189.59

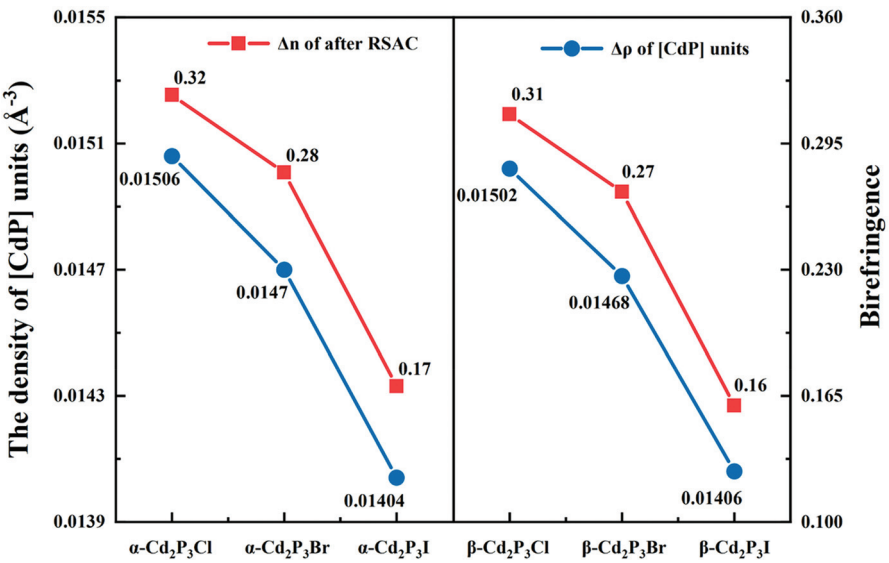

Fig. 2 The [CdP] unit density of the corresponding compounds and the birefringence after RSAC.

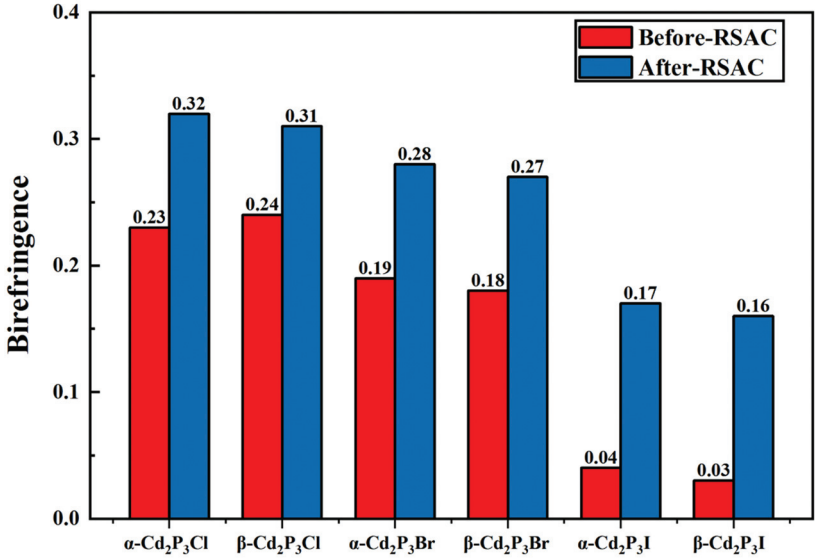

Fig. 3 Comparison of birefringence before and after by RSAC of α-Cd_2P_3X (X = Cl, Br, and I) and β-Cd_2P_3X (X = Cl, Br, and I).

birefringence. The Born effective charge tensor was calculated, which could directly illustrate the microscopic origin of the birefringence. The formula could be written as

$$q_{ij}^{\text{Born}} = \left(\frac{\Omega}{e}\right)\frac{\delta p_i}{\delta d_j}$$

in which q_{ij}^{Born} is the Born effective charge, Ω is the unit cell volume, e is the electronic charge, and δp_i is the change in polarization along the displacement direction δd_j. The Born effective charges of each atom in α-Cd_2P_3Cl are listed in Table 2. It is obvious that the Cl atoms have the largest value of Δq, which means that the Cl atoms have the strongest influence on the birefringence. The influence of halogens in other compounds on birefringence is the same as that in α-Cd_2P_3Cl, and the calculated results for other compounds are shown in Table S7 in the ESI.† The results also reflect that the Born effective charges increased from Cl to Br to I, and are 0.808, 1.011, and 1.302 in α-Cd_2P_3X (X = Cl, Br, and I), respectively. The increase in Δq is mainly caused by the intensified electron distribution, which becomes more and more susceptible to polarization and sensitive to birefringence.

The birefringence originates from the structural anisotropy and at the microscale, it originates from the polarizability anisotropy ($\Delta\alpha$) of fundamental building blocks (FBBs). Herein, how halogen atoms adjust the $\Delta\alpha$ value of FBBs is analyzed. The $\Delta\alpha$ values can be acquired from static polarization according to the following formula:[23]

$$\Delta\alpha = \sqrt{\left[(\alpha_{xx}-\alpha_{yy})^2+(\alpha_{xx}-\alpha_{zz})^2+(\alpha_{yy}-\alpha_{zz})^2+6(\alpha_{xy}{}^2+\alpha_{xz}{}^2+\alpha_{yz}{}^2)^2\right]/2}$$

where α is static polarization and $\Delta\alpha$ is polarizability anisotropy. The $\Delta\alpha$ values of the $[CdP_3X]/[CdP_3X_2]$ groups

Table 2 Born effective charges of α-Cd_2P_3X (X = Cl, Br, and I) under DFPT calculations

Compounds	Atoms	q_{xx}	q_{yy}	q_{zz}	Δq
α-Cd_2P_3Cl	Cd_1	2.264	2.178	2.175	−0.002
	Cd_2	2.285	2.174	2.190	0.016
	Cl	−1.998	−1.879	−1.071	0.808
	P_1	−0.876	−0.811	−1.418	−0.607
	P_2	−0.786	−0.831	−0.440	0.391
	P_3	−0.890	−0.830	−1.437	−0.607

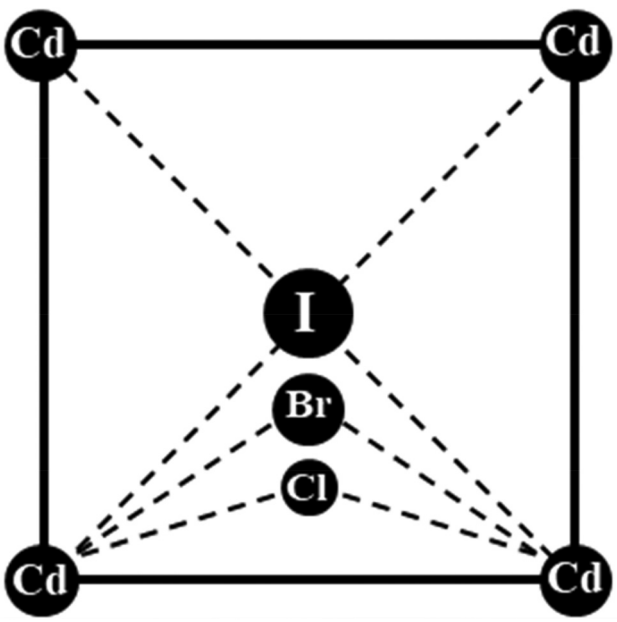

Fig. 4 The schematic diagram of the coordination of halogens with adjacent Cd atoms.

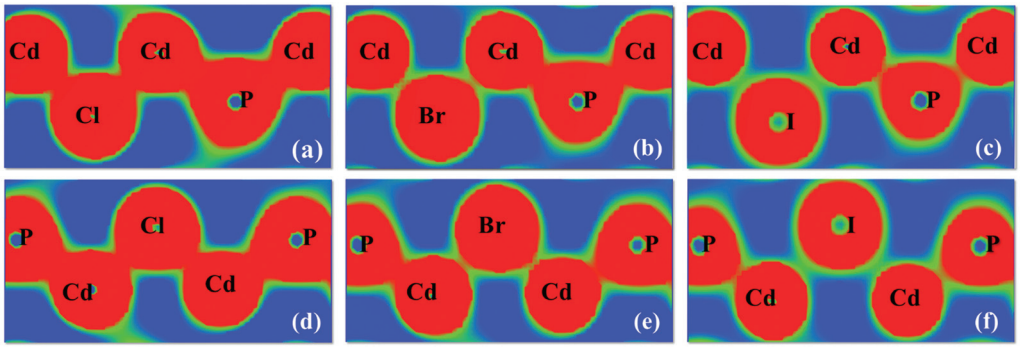

Fig. 5 Electron density maps of α-Cd_2P_3X (X = Cl, Br, and I) (a–c), and β-Cd_2P_3X (X = Cl, Br, and I) (d–f).

decrease from Cl to I (as shown in Table 2). Taking the α-Cd_2P_3X (X = Cl, Br, and I) series as the examples, the $\Delta\alpha$ values are 125.47 ($[Cd^IP_3Cl]$), 103.28 ($[Cd^IP_3Br_2]$) and 45.89 ($[Cd^IP_3I_2]$). The differences could be glimpsed from the structural perspective. As shown in Fig. 1c, in the structures of α-Cd_2P_3X (X = Cl, Br, and I), the Cd–P framework is planar, and has large anisotropy. The insertion of halogen atoms between the layers will absolutely decrease the whole anisotropy. Besides, the Cd–X bond lengths increase from Cl to Br to I, which renders the halogen atom closer to the center of the four surrounding Cd atoms (Fig. 4), and finally weakens the anisotropy as a whole. From the charge density diagram (Fig. 5), it could be obviously seen that the electron cloud distributions between Cd and the halogens are more and more dispersive from Cl to Br to I, which form weaker interactions and show a decreasing trend of $\Delta\alpha$ of $[CdP_3X]/[CdP_3X_2]$ polyhedra.

The contribution of Cd to optical properties is not ignored. Fig. S3† displays the electron-density difference map for α-Cd_2P_3Cl. This clearly reveals that the highly asymmetric electron distribution of the Cd^{2+} cations influences the optical anisotropy.[68]

4. Conclusion

In summary, we have successfully studied the optical properties and explored the contributions of microscopic groups to optical anisotropy and NLO response on the crystal structure of the synthesized cadmium phosphohalides. Through the first-principles, real-space atom-cutting, and polarization anisotropy analysis methods, it was found that halogens can obviously influence the optical properties and modulate the polarizability anisotropy of the polyhedral active group by the synergistic effect of anion size and covalent interactions. This work provides an afflatus for the comprehension of the optical anisotropy origin mechanism.

Conflicts of interest

The authors declare that they have no conflict of interest.

Acknowledgements

This work is supported by the National Natural Science Foundation of China (Grant No. 11864039).

Notes and references

1 (*a*) K. M. Ok, Toward the Rational Design of Novel NoncentroSymmetric Materials: Factors Influencing the Framework Structures, *Acc. Chem. Res.*, 2016, **49**, 2774–2785; (*b*) T. T. Tran, H. W. Yu, J. M. Rondinelli, K. R. Poeppelmeier and P. S. Halasyamani, Deep ultraviolet nonlinear optical materials, *Chem. Mater.*, 2016, **28**, 5238–5258.

2 (*a*) X. L. Chen, H. Jo and K. M. Ok, Lead Mixed Oxyhalides Satisfying All Fundamental Requirements for High–Performance Mid–Infrared Nonlinear Optical Materials, *Angew. Chem., Int. Ed.*, 2020, **59**, 7514–7520; (*b*) X. Su, Z. H. Yang, G. P. Han, Y. Wang, M. Wen and S. L. Pan, Role of the Metal Cation Types around VO_4 Groups on the Nonlinear Optical Behavior of Materials: Experimental and Theoretical Analysis, *Dalton Trans.*, 2016, **45**, 14394–14402.

3 K. M. Ok, E. O. Chi and P. S. Halasyamani, Bulk Characterization Methods for Non-Centrosymmetric Materials: Second-Harmonic Generation, Piezoelectricity, Pyroelectricity, and Ferroelectricity, *Chem. Soc. Rev.*, 2006, **35**, 710–717.

4 X. L. Chen, Q. Jing and K. M. Ok, $Pb_{18}O_8Cl_{15}I_5$: A Polar Lead Mixed Oxyhalide with Unprecedented Architecture and Excellent Infrared Nonlinear Optical Properties, *Angew. Chem., Int. Ed.*, 2020, **59**, 20323–20327.

5 Z. H. Yang, A. Tudi, B. H. Lei and S. L. Pan, Enhanced Nonlinear Optical Functionality in Birefringence and Refractive Index Dispersion of the Deep-Ultraviolet Fluorooxoborates, *Sci. China Mater.*, 2020, **63**, 1480–1488.

6 C. Hu, B. B. Zhang, B. H. Lei, S. L. Pan and Z. H. Yang, Advantageous Units in Antimony Sulfides: Exploration and Design of Infrared Nonlinear Optical Materials, *ACS Appl. Mater. Interfaces*, 2018, **10**, 26413–26421.

7 (*a*) M. Mutailipu, M. Zhang, B. B. Zhang, L. Y. Wang, Z. H. Yang, X. Zhou and S. L. Pan, $SrB_5O_7F_3$ Functionalized with $B_5O_9F_3^{6-}$ Chromophores: Accelerating the Rational Design of Deep-Ultraviolet Nonlinear Optical Materials, *Angew. Chem., Int. Ed.*, 2018, **57**, 6095–6099; (*b*) M. Zhang, X. Su, S. L. Pan, Z. Wang, H. Zhang, Z. H. Yang, B. B. Zhang, L. Y. Dong, Y. Wang, F. F. Zhang and Y. Yang, Linear and Nonlinear Optical Properties of $K_3B_6O_{10}Br$ Single Crystal: Experiment and Calculation, *J. Phys. Chem. C*, 2014, **118**, 11849–11856.

8 H. P. Wu, S. L. Pan, K. R. Poeppelmeier, H. Y. Li, D. Z. Jia, Z. H. Chen, X. Y. Fan, Y. Yang, J. M. Rondinelli and H. S. Luo, $K_3B_6O_{10}Cl$: A New Structure Analogous to Perovskite with a Large Second Harmonic Generation Response and Deep UV Absorption Edge, *J. Am. Chem. Soc.*, 2011, **133**, 7786–7790.

9 H. P. Wu, H. W. Yu, Z. H. Yang, X. L. Hou, X. Su, S. L. Pan, K. R. Poeppelmeier and J. M. Rondinelli, Designing a Deep-ultraviolet Nonlinear Optical Material with a Large Second Harmonic Generation Response, *J. Am. Chem. Soc.*, 2013, **135**, 4215–4218.

10 M. Luo, F. Liang, Y. X. Song, D. Zhao, N. Ye and Z. S. Lin, Rational Design of the First Lead/Tin Fluorooxoborates $MB_2O_3F_2$ (M = Pb, Sn), Containing Flexible Two-Dimensional $[B_6O_{12}F_6]_\infty$ Single Layers with Widely Divergent Second Harmonic Generation Effects, *J. Am. Chem. Soc.*, 2018, **140**, 6814–6817.

11 (*a*) W. G. Zhang, H. W. Yu, H. P. Wu and P. S. Halasyamani, Phase-Matching in Nonlinear Optical Compounds: A Materials Perspective, *Chem. Mater.*, 2017, **29**, 2655–2668; (*b*) P. S. Halasyamani and W. G. Zhang, Viewpoint: Inorganic Materials for UV and Deep-UV Nonlinear-Optical Applications, *Inorg. Chem.*, 2017, **56**, 12077–12085.

12 (*a*) M. Mutailipu, M. Zhang, Z. H. Yang and S. L. Pan, Targeting the Next Generation of Deep-ultraviolet Nonlinear Optical Materials: Expanding from Borates to Borate Fluorides to Fluorooxoborates, *Acc. Chem. Res.*, 2019, **52**, 791–801; (*b*) Q. Bian, Z. H. Yang, L. Y. Dong, S. L. Pan, H. Zhang, H. P. Wu, H. W. Yu, W. W. Zhao and Q. Jing, First Principle Assisted Prediction of the Birefringence Values of Functional Inorganic Borate Materials, *J. Phys. Chem. C*, 2014, **118**, 25651–25657.

13 L. Kang, M. L. Zhou, J. Y. Yao, Z. S. Lin, Y. C. Wu and C. T. Chen, Metal Thiophosphates with Good Mid-Infrared Nonlinear Optical Performances: A First-Principles Prediction and Analysis, *J. Am. Chem. Soc.*, 2015, **137**, 13049–13059.

14 M. Mutailipu and S. L. Pan, Emergent Deep-ultraviolet Nonlinear Optical Candidates, *Angew. Chem., Int. Ed.*, 2020, **59**, 20302–20317.

15 G. Q. Zhou, J. Xu, X. D. Chen, H. Y. Zhong, S. T. Wang, K. Xu, P. Z. Deng and F. X. Gan, Growth and Spectrum of a Novel Birefringent α-BaB_2O_4 Crystal, *J. Cryst. Growth*, 1998, **191**, 517–519.

16 H. T. Luo, T. Tkaczyk, E. L. Dereniak, K. Oka and R. Sampson, High Birefringence of the Yttrium Vanadate Crystal in the Middle Wavelength Infrared, *Opt. Lett.*, 2006, **31**, 616–618.

17 G. Ghosh, Dispersion-equation Coefficients for the Refractive Index and Birefringence of Calcite and Quartz Crystals, *Opt. Commun.*, 1999, **163**, 95–102.

18 J. R. Devore, Refractive Indices of Rutile and Sphalerite, *J. Opt. Soc. Am.*, 1951, **41**, 416–419.

19 M. J. Dodge, Refractive Properties of Magnesium Fluoride, *Appl. Opt.*, 1984, **23**, 1980–1985.

20 X. L. Chen, B. B. Zhang, F. F. Zhang, Y. Wang, M. Zhang, Z. H. Yang, K. R. Poeppelmeier and S. L. Pan, Designing an Excellent Deep-Ultraviolet Birefringent Material for Light Polarization, *J. Am. Chem. Soc.*, 2018, **140**, 16311–16319.

21 M. Zhang, D. An, C. Hu, X. L. Chen, Z. H. Yang and S. L. Pan, Rational Design via Synergistic Combination Leads to an Outstanding Deep-Ultraviolet Birefringent $Li_2Na_2B_2O_5$ Material with an Unvalued B_2O_5 Functional Gene, *J. Am. Chem. Soc.*, 2019, **141**, 3258–3264.

22 J. B. Huang, J. N. Cheng, B. H. Lei, Z. L. Wei, S. L. Pan and Z. H. Yang, Synergism of Multiple Functional Chromophores Significantly Enhancing the Birefringence in Layered Non-Centrosymmetric Chalcohalides, *Inorg. Chem. Front.*, 2021, **8**, 1588–1598.

23 T. H. Tong, W. Y. Zhang, Z. H. Yang and S. L. Pan, Series of Crystals with Giant Optical Anisotropy: A Targeted Strategic Research, *Angew. Chem., Int. Ed.*, 2020, **60**, 1332–1338.

24 J. Lu, Y. K. Lian, L. Xiong, Q. R. Wu, M. Zhao, K. X. Shi, L. Chen and L. M. Wu, How to Maximize Birefringence and Nonlinearity of π-Conjugated Cyanurates, *J. Am. Chem. Soc.*, 2019, **141**, 16151–16159.

25 F. Kong, C. L. Hu, M. L. Liang and J. G. Mao, $Pb_4(OH)_4(BrO_3)_3(NO_3)$: An Example of SHG Crystal in Metal Bromates Containing π-Conjugated Planar Triangle, *Inorg. Chem.*, 2016, **55**, 948–955.

26 Y. C. Liu, Y. G. Shen and S. G. Zhao, Structure-Property Relationship in Nonlinear Optical Materials with π-conjugated CO_3 Triangles, *Coord. Chem. Rev.*, 2020, **407**, 213152–213172.

27 (*a*) Y. G. Shen, S. G. Zhao and J. H. Luo, The Role of Cations in Second-Order Nonlinear Optical Materials Based on π-conjugated $[BO_3]^{3-}$ Groups, *Coord. Chem. Rev.*, 2018, **366**, 1–28; (*b*) S. Y. Zhang, X. Wu, Y. T. Song, D. Q. Ni, B. Q. Hu and T. Zhou, Growth of Birefringent $Ca_3(BO_3)_2$ Crystals by the Czochralski Method, *J. Cryst. Growth*, 2003, **252**, 246–250.

28 D. H. Lin, M. Luo, C. S. Lin, F. Xu and N. Ye, KLi$(HC_3N_3O_3)\cdot 2H_2O$: Solvent-Drop Grinding Method Toward the Hydro-Isocyanurate Nonlinear Optical Crystal, *J. Am. Chem. Soc.*, 2019, **141**, 3390–3394.

29 G. Q. Shi, Y. Wang, F. F. Zhang, B. B. Zhang, Z. H. Yang, X. L. Hou, S. L. Pan and K. R. Poeppelmeier, Finding the Next Deep-Ultraviolet Nonlinear Optical Material: $NH_4B_4O_6F$, *J. Am. Chem. Soc.*, 2017, **139**, 10645–10648.

30 Z. Z. Zhang, Y. Wang, B. B. Zhang, Z. H. Yang and S. L. Pan, Polar Fluorooxoborate, NaB_4O_6F: A Promising

Material for Ionic Conduction and Nonlinear Optics, *Angew. Chem., Int. Ed.*, 2018, **57**, 6577–6581.

31 X. F. Wang, Y. Wang, B. B. Zhang, F. F. Zhang, Z. H. Yang and S. L. Pan, CsB_4O_6F: A Congruent–Melting Deep–Ultraviolet Nonlinear Optical Material by Combining Superior Functional Units, *Angew. Chem., Int. Ed.*, 2017, **56**, 14119–14123.

32 Y. Wang, B. B. Zhang, Z. H. Yang and S. L. Pan, Cation–Tuned Synthesis of Fluorooxoborates: Towards Optimal Deep–Ultraviolet Nonlinear Optical Materials, *Angew. Chem., Int. Ed.*, 2018, **57**, 2150–2154.

33 (*a*) R. Gautier, R. G. Gautier, K. B. Chang and K. R. Poeppelmeier, On the Origin of the Differences in Structure Directing Properties of Polar Metal Oxyfluoride $[MO_xF_{6-x}]^{2-}$ (x = 1, 2) Building Units, *Inorg. Chem.*, 2015, **54**, 1712–1719; (*b*) H. Kimura, H. Koizumi, T. Uchida and S. Uda, Influence of Impurity Doping on the Partitioning of Intrinsic Ionic Species during the Growth of $LiNbO_3$ Crystal from the Melt, *J. Cryst. Growth*, 2009, **311**, 1553–1558.

34 J. D. Bierlein and H. Vanherzeele, Potassium Titanyl Phosphate: Properties and New Applications, *J. Opt. Soc. Am. B*, 1989, **6**, 622–633.

35 J. Y. Guo, A. Tudi, S. J. Han, Z. H. Yang and S. L. Pan, α-SnF_2: A UV Birefringent Material with Large Birefringence and Easy Crystal Growth, *Angew. Chem., Int. Ed.*, 2021, **60**, 3540–3544.

36 J. Y. Guo, A. Tudi, S. J. Han, Z. H. Yang and S. L. Pan, $Sn_2B_5O_9Cl$: A Material with Large Birefringence Enhancement Activated Prepared via Alkaline-Earth-Metal Substitution by Tin, *Angew. Chem., Int. Ed.*, 2019, **58**, 17675–17678.

37 J. Y. Guo, S. C. Cheng, S. J. Han, Z. H. Yang and S. L. Pan, $Sn_2B_5O_9Br$ as an Outstanding Bifunctional Material with Strong Second–Harmonic Generation Effect and Large Birefringence, *Adv. Opt. Mater.*, 2021, **9**, 2001734–2001740.

38 B. L. Wu, C. L. Hu, F. F. Mao, R. L. Tang and J. G. Mao, Highly Polarizable Hg^{2+} Induced a Strong Second Harmonic Generation Signal and Large Birefringence in $LiHgPO_4$, *J. Am. Chem. Soc.*, 2019, **141**, 10188–10192.

39 C. Li, W. L. Yin, P. F. Gong, X. S. Li, M. L. Zhou, A. Mar, Z. S. Lin, J. Y. Yao, Y. C. Wu and C. T. Chen, Trigonal Planar $[HgSe_3]^{4-}$ Unit: A New Kind of Basic Functional Group in IR Nonlinear Optical Materials with Large Susceptibility and Physicochemical Stability, *J. Am. Chem. Soc.*, 2016, **138**, 6135–6138.

40 Z. Li, Y. Yang, Y. W. Guo, W. H. Xing, X. Y. Luo, Z. S. Lin, J. Y. Yao and Y. C. Wu, Broadening Frontiers of Infrared Nonlinear Optical Materials with π-conjugated Trigonal-Planar Groups, *Chem. Mater.*, 2019, **31**, 1110–1117.

41 Y. C. Liu, X. M. Liu, S. Liu, Q. R. Ding, Y. Q. Li, L. N. Li, S. G. Zhao, Z. S. Lin, J. H. Luo and M. C. Hong, An Unprecedented Antimony(III) Borate with Strong Linear and Nonlinear Optical Responses, *Angew. Chem., Int. Ed.*, 2020, **59**, 7793–7796.

42 J. Beck, S. Hedderich and K. Köllisch, Hg_3AsE_4X (E = S, Se; X = Cl, Br, I), A Family of Isotypic Compounds with an Acentric, Layered Structure, *Inorg. Chem.*, 2000, **39**, 5847–5850.

43 S. Liu, X. M. Liu, S. G. Zhao, Y. C. Liu, L. N. Li, Q. R. Ding, Y. Q. Li, Z. S. Lin, J. H. Luo and M. C. Hong, An Exceptional Peroxide Birefringent Material Resulting from d-π Interactions, *Angew. Chem., Int. Ed.*, 2020, **59**, 9414–9417.

44 (*a*) A. Rebbah, J. Yazbeck, R. Lande and A. Deschanvres, Etudes structurales et optiques des phases du type Cd_2A_3X (A = As, P; X = Cl, Br, I) et de leur solution solide, *Mater. Res. Bull.*, 1981, **16**, 525–533; (*b*) P. C. Donohue, The Synthesis and Properties of Cd_2P_3Cl, Cd_2P_3Br, and Cd_2P_3I, *J. Solid State Chem.*, 1972, **5**, 71–74; (*c*) A. Roy, A. Singh, S. A. Aravindh, S. Servottam, U. V. Waghmare and C. N. R. Rao, Structural Features and HER activity of Cadmium Phosphohalides, *Angew. Chem., Int. Ed.*, 2019, **58**, 6926–6931.

45 N. A. Spaldin, A Beginner's Guide to the Modern Theory of Polarization, *J. Solid State Chem.*, 2012, **195**, 2–10.

46 J. N. Cheng, B. H. Lei, C. Zhou, S. L. Pan and Z. H. Yang, Adjustable Optical Nonlinearity in d^{10} Cations Containing Chalcogenides via dp Hybridization Interaction, *Dalton Trans.*, 2019, **48**, 2592–2597.

47 Q. Q. Zhang, Q. Jing, H. M. Duan and H. B. Cao, The Relationship between Covalent Bonds and the Optical Response in a Nonpolar Family $ATeMoO_6$ (A = Mg, Zn, Cd): A Berry-Phase investigation, *J. Solid State Chem.*, 2018, **264**, 22–28.

48 Q. Jing, G. Yang, J. Hou, M. Z. Sun and H. B. Cao, Positive and Negative Contribution to Birefringence in a Family of Carbonates: A Born Effective Charges Analysis, *J. Solid State Chem.*, 2016, **244**, 69–74.

49 L. J. Sham and M. Schluter, Density-Functional Theory of the Energy Gap, *Phys. Rev. Lett.*, 1983, **51**, 1888–1891.

50 S. J. Clark, M. D. Segall, C. J. Pickard, P. J. Hasnip, M. J. Probert, K. Refson and M. C. Payne, First Principles Methods Using CASTEP, *Z. Kristallogr. – Cryst. Mater.*, 2005, **220**, 567–570.

51 J. P. Perdew, K. Burke and M. Ernzerhof, Generalized Gradient Approximation Made Simple, *Phys. Rev. Lett.*, 1996, **77**, 3865–3868.

52 A. M. Rappe, K. M. Rabe, E. Kaxiras and J. D. Joannopoulos, Optimized Pseudopotentials, *Phys. Rev. B: Condens. Matter Mater. Phys.*, 1990, **41**, 1227–1230.

53 C. Aversa and J. E. Sipe, Nonlinear Optical Susceptibilities of Semiconductors: Results with a Length-Gauge Analysis, *Phys. Rev. B: Condens. Matter Mater. Phys.*, 1995, **52**, 14636–14645.

54 B. B. Zhang, M. H. Lee, Z. H. Yang, Q. Jing, S. L. Pan, M. Zhang, H. P. Wu, X. Su and Z. X. Li, Simulated Pressure-Induced Blue-Shift of Phase-Matching Region and Nonlinear Optical Mechanism for $K_3B_6O_{10}X$ (X = Cl, Br), *Appl. Phys. Lett.*, 2015, **106**, 031906–031912.

55 A. V. Shevelkov, E. V. Dikarev and B. A. Popovkin, Helical $^1{}_\infty$Chains in the Structures of Hg_2P_3Br and Hg_2P_3Cl, *Z. Kristallogr.*, 1994, **209**, 583–585.

56 A. V. Krukau, O. A. Vydrov, A. F. Izmaylov and G. E. Scuseria, Influence of the exchange screening parameter on the performance of screened hybrid functionals, *J. Chem. Phys.*, 2006, **125**, 224106–224111.

57 A. V. Krukau, O. A. Vydrov, A. F. Izmaylov and G. E. Scuseria, Influence of the Exchange Screening Parameter on the Performance of Screened Hybrid Functionals, *J. Chem. Phys.*, 2006, **125**, 224106–2241012.

58 (*a*) B. B. Zhang, G. Q. Shi, Z. H. Yang, F. F. Zhang and S. L. Pan, Fluorooxoborates: Beryllium-Free Deep-Ultraviolet Nonlinear Optical Materials without Layered Growth, *Angew. Chem., Int. Ed.*, 2017, **56**, 3916–3919; (*b*) Y. Wang and S. L. Pan, Recent Development of Metal Borate Halides: Crystal Chemistry and Application in Second-Order NLO Materials, *Coord. Chem. Rev.*, 2016, **323**, 15–35.

59 (*a*) X. Shi, Z. Ma, C. He and K. Wu, Strong SHG Responses Predicted in Binary Metal Halide Crystal HgI_2, *Chem. Phys. Lett.*, 2014, **608**, 219–223; (*b*) P. F. Gong, F. Liang, L. Kang, X. G. Chen, J. G. Qin, Y. C. Wu and Z. S. Lin, Recent Advances and Future Perspectives on Infrared Nonlinear Optical Metal Halides, *Coord. Chem. Rev.*, 2019, **380**, 83–102; (*c*) T. Liu, J. G. Qin, G. Zhang, T. Zhu, F. Niu, Y. Wu and C. Chen, Mercury Bromide ($HgBr_2$): A Promising Nonlinear Optical Material in IR Region with a High Laser Damage Threshold, *Appl. Phys. Lett.*, 2008, **93**, 091102–091106.

60 (*a*) C. Barta and C. Barta Jr., Physical Properties of Single Crystals of the Calomel Gorup (Hg_2X_2: X = Cl, Br)[1], *Mater. Sci. Forum*, 1991, **61**, 93–150; (*b*) R. Z. Li, G. D. Zhang, L. Liu, L. Z. Zhang, P. Zhang, X. Li and Y. Q. Hua, Origin of Ultra-Wide IR Transmission and Ultra-Large Birefringence of Mercurous Halide Series with One Dimensional Chain-Like Structure: An ab Initio Study, *Comput. Mater. Sci.*, 2020, **188**, 110139–110147; (*c*) P. M. Amarasinghe, J. S. Kim, F. Jin, S. Trivedi, S. B. Qadri, J. Feng, J. Soos, M. Diestler, N. Gupta and J. L. Jensen, Anomalous Thermal Expansion of Mercurous Halides, in *Infrared Sensors, Devices, and Application VIII*, Int. Soc. Opt. Photon., 2018, vol. 10766, p. 107660M; (*d*) L. Van den Berg, Growth of Single Crystals of Mercuric Iodide on the Ground and in Space, *Mater. Res. Soc. Symp. Proc.*, 1993, **302**, 73–78.

61 (*a*) L. C. Tang, J. Y. Huang, C. S. Chang, M. H. Lee and L. Q. Liu, New Infrared Nonlinear Optical Crystal $CsGeBr_3$: Synthesis, Structure and Powder Second-Harmonic Generation Properties, *J. Phys.: Condens. Matter*, 2005, **17**, 7275–7286; (*b*) C. C. Stoumpos, L. Frazer, D. J. Clark, Y. S. Kim, S. H. Rhim, A. J. Freeman, J. B. Ketterson, J. I. Jang and M. G. Kanatzidis, Hybrid Germanium Iodide Perovskite Semiconductors: Active Lone Pairs, Structural Distortions, Direct and Indirect Energy Gaps, and Strong Nonlinear Optical Properties, *J. Am. Chem. Soc.*, 2015, **137**, 6804–6819; (*c*) R. J. Sutton, M. R. Filip, A. A. Haghighirad, N. Sakai, B. Wenger, F. Giustino and H. J. Snaith, Cubic or Orthorhombic? Revealing the Crystal Structure of Metastable Black-Phase $CsPbI_3$ by Theory and Experiment, *ACS Energy Lett.*, 2018, **3**, 1787–1794; (*d*) M. R. Linaburg, E. T. McClure, J. D. Majher and P. M. Woodward, $Cs_{1-x}Rb_xPbCl_3$ and $Cs_{1-x}Rb_xPbBr_3$ Solid Solutions: Understanding Octahedral Tilting in Lead Halide Perovskites, *Chem. Mater.*, 2017, **29**, 3507–3514; (*e*) T. T. Tong, M. H. Lee and J. Zhang, Transformation of Optical Anisotropy Origins in Perovskite-Related Materials: A First-Principles Study, *J. Phys. Chem. C*, 2019, **123**, 31167–31174.

62 (*a*) L. Gao, J. B. Huang, S. R. Guo, Z. H. Yang and S. L. Pan, Structure-Property Survey and Computer-Assisted Screening of Mid-Infrared Nonlinear Optical Chalcohalides, *Coord. Chem. Rev.*, 2020, **421**, 213379–213399; (*b*) P. Schwarz, J. Wachter and M. Zabel, PAs_3S_3 cage as a new building block in copper halide coordination polymers, *Inorg. Chem.*, 2011, **50**, 8477–8483.

63 (*a*) G. Zhang, J. G. Qin, T. Liu, Y. J. Li, Y. C. Wu and C. T. Chen, $NaSb_3F_{10}$: A New Second-Order Nonlinear Optical Crystal to be Used in the IR Region with Very High Laser Damage Threshold, *Appl. Phys. Lett.*, 2009, **95**, 261104–261104; (*b*) L. Kang, D. M. Ramo, Z. S. Lin, P. D. Bristowe, J. G. Qin and C. T. Chen, First Principles Selection and Design of Mid-IR Nonlinear Optical Halide Crystals, *J. Mater. Chem. C*, 2013, **1**, 7363–7370.

64 G. Zhang, T. Liu, T. X. Zhu, J. G. Qin, Y. C. Wu and C. T. Chen, SbF_3: A New Second-Order Nonlinear Optical Material, *Opt. Mater.*, 2008, **31**, 110–113.

65 (*a*) Y. Z. Huang, L. M. Wu, X. T. Wu, L. H. Li, L. Chen and Y. F. Zhang, $Pb_2B_5O_9I$: An Iodide Borate with Strong Second Harmonic Generation, *J. Am. Chem. Soc.*, 2010, **132**, 12788–12789; (*b*) E. L. Belokoneva, A. G. Al-Ama, S. Y. Stefanovich and P. A. Plachinda, Crystal Structure of the Lead Bromo-Borate $Pb_2[B_5O_9]Br$ from Precision Single-Crystal X-ray Diffraction Data and the Problem of Optical Nonlinearity of Hilgardites, *Crystallogr. Rep.*, 2007, **52**, 795–800; (*c*) O. Ferro, S. Merlino, S. A. Vinogradova, D. Y. Pushcharovsky and O. V. Dimitrova, Crystal Structures of Two New Ba Borates Pentaborate, Ba_2 $[B_5O_9]Cl{\cdot}0.5H_2O$ and $Ba_2[B_5O_8(OH)_2](OH)$, *J. Alloys Compd.*, 2000, **305**, 63–71; (*d*) S. Ghose and C. Wan, Hilgardite, $Ca_2[B_5O_9]Cl{\cdot}H_2O$: A Piezoelectric Zeolite-Type Pentaborate, *Am. Mineral.*, 1979, **64**, 187–195; (*e*) Q. Wei, J. W. Cheng, C. He and G. Y. Yang, An Acentric Calcium Borate $Ca_2[B_5O_9]{\cdot}(OH){\cdot}H_2O$: Synthesis, Structure, and Nonliner Optical Property, *Inorg. Chem.*, 2014, **53**, 11757–11763.

66 X. Y. Zhou, J. B. Huang, G. M. Cai, H. W. Zhou, Y. N. Huang and X. Su, Large Optical Polarizability Causing Positive Effects on the Birefringence of Planar-Triangular BO_3 Groups in Ternary Borates, *Dalton Trans.*, 2020, **49**, 3284–3292.

67 (*a*) J. Lin, M. H. Lee, Z. P. Liu, C. T. Chen and C. J. Pickard, Mechanism for Linear and Nonlinear Optical Effects in β-BaB_2O_4 Crystals, *Phys. Rev. B: Condens. Matter Mater. Phys.*, 1999, **60**, 13380–13390; (*b*) L. Gao, T. H. Tong, K. W. Zhang and J. Zhang, Hierarchical Contribution of Anions to Second Harmonic Generation in A_2HgI_4 (A = Na,

Ag, Cu) Regulated Dramatically by Metal Cations, *Cryst. Growth Des.*, 2020, **20**, 7470–7476.

68 Y. L. Deng, L. Huang, X. H. Dong, L. Wang, K. M. Ok, H. M. Zeng, Z. E. Lin and G. H. Zou, $K_2Sb(P_2O_7)F$: Unprecedented Cairo Pentagonal Layer with New Bifunctional Genes Revealing Excellent Optical Performance, *Angew. Chem., Int. Ed.*, 2020, **59**, 21151–21156.